Gait & Posture 112 (2024) 8–15

Contents lists available at ScienceDirect

Gait & Posture

journal homepage: www.elsevier.com/locate/gaitpost

Hindfoot kinematics and kinetics - A combined *in vivo* and *in silico* analysis approach

Barbara Postolka [a,*,1], Bryce A. Killen [a,1], Hannelore Boey [a,b,2], Tiago M. Malaquias [b,3], Tassos Natsakis [b,c], Stefan Clockaerts [d], Dominique Misselyn [e], Walter Coudyzer [f], Jos Vander Sloten [b], Ilse Jonkers [a]

[a] KU Leuven, Department of Movement Sciences, Human Movement Biomechanics Research Group, Tervuursevest 101, Leuven 3001, Belgium
[b] KU Leuven, Department of Mechanical Engineering, Biomechanics Section, Celestijnenlaan 300C, Leuven 3001, Belgium
[c] Technical University of Cluj-Napoca, Department of Automation, Dorobantilor 71-73, Cluj-Napoca 400268, Romania
[d] Holy Heart Hospital Lier, Department of Orthopaedic Surgery and Traumatology, Mechelsesteenweg 24, Lier 2500, Belgium
[e] UZ Leuven, Department of Development and Regeneration, Herestraat 49, Leuven 3000, Belgium
[f] UZ Leuven, Radiology, Herestraat 49, Leuven 3000, Belgium

ARTICLE INFO

Keywords:
4D CT
Foot-ankle complex
Talocrural joint
Subtalar joint
Articular joint mechanics
Hindfoot

ABSTRACT

Background: The complex anatomical structure of the foot-ankle imposes challenges to accurately quantify detailed hindfoot kinematics and estimate musculoskeletal loading parameters. Most systems used to capture or estimate dynamic joint function oversimplify the anatomical structure by reducing its complexity.
Research Question: Can four dimensional computed tomography (4D CT) imaging in combination with an innovative foot manipulator capture in vivo hindfoot kinematics during a simulated stance phase of walking and can talocrural and subtalar articular joint mechanics be estimated based on a detailed in silico musculoskeletal foot-ankle model.
Methods: A foot manipulator imposed plantar/dorsiflexion and inversion/eversion representing a healthy stance phase of gait in 12 healthy participants while simultaneously acquiring 4D CT images. Participant-specific 3D hindfoot rotations and translations were calculated based on bone-specific anatomical coordinate systems. Articular cartilage contact area and contact pressure of the talocrural and subtalar joints were estimated using an extended foot-ankle model updated with an elastic foundation contact model upon prescribing the participant-specific rotations measured in the 4D CT measurement.
Results: Plantar/dorsiflexion predominantly occurred at the talocrural joint (RoM 15.9±3.9°), while inversion/eversion (RoM 5.9±3.9°) occurred mostly at the subtalar joint, with the contact area being larger at the subtalar than at the talocrural joint. Contact pressure was evenly distributed between the talocrural and subtalar joint at the beginning of the simulated stance phase but was then redistributed from the talocrural to the subtalar joint with increasing dorsiflexion.
Significance: In a clinical case study, the healthy participants were compared with four patients after surgically treaded intra-articular calcaneal fracture. The proposed workflow was able to detect small but meaningful differences in hindfoot kinematics and kinetics, indicative of remaining hindfoot pathomechanics that may influence the onset and progression of degenerative joint diseases.

1. Background

The foot-ankle complex connects the human body to the ground and plays an important role in weight-bearing and lower limb propulsion during locomotion. Knowledge of kinematics and kinetics of individual foot-ankle joints can provide information about foot function and as

* Corresponding author.
E-mail address: barbara.postolka@kuleuven.be (B. Postolka).
[1] Joint first author
[2] Present address: Thomas More, Mobilab & Care, Kleinhoefstraat 4, 2440 Geel, Belgium
[3] Present address: STATSports Group Limited, Drumalane Mill, BT35 8QS Newry, Northern Ireland, UK

https://doi.org/10.1016/j.gaitpost.2024.04.023
Received 1 December 2023; Received in revised form 13 March 2024; Accepted 23 April 2024
Available online 26 April 2024

such inform about joint-related musculoskeletal pathologies or effects of conservative or surgical treatment methods.

Three dimensional (3D) motion-capture using detailed skin marker models is a frequently used technology in clinical practice to quantify foot-ankle kinematics. While these systems enable *in vivo* assessment during a wide range of activities, their accuracy is limited by soft-tissue artefacts [1]. Quantification of foot-ankle motion is further complicated by the fact that most marker models measure the movement of rigid foot segments combining multiple bones rather than the movement of individual bones and therefore simplify the kinematic description of the foot-ankle complex [2,3]. In particular, the talus, which plays an important role in hindfoot motion as part of the talocrural (tibio-talar) and subtalar (talo-calcaneal) joints, is not accessible by skin marker analysis and therefore its movement can only be inferred based on the relative movement of the tibia and calcaneus [2–4]. To overcome these limitations and directly measure 3D bone orientation and location, medical imaging can be used. Magnetic resonance imaging (MRI), computed tomography (CT), and more recently weight-bearing CT allow accurate imaging of individual foot bones and are often used in clinical routine. While these medical imaging systems are limited to acquisitions of static positions, dynamic videofluoroscopy [5,6] allows to assess *in vivo* bone motion during dynamic activities. Bi-plane videofluoroscopy has been successfully used to study hindfoot kinematics during gait-like activities [7–10] and highlighted the importance of quantifying all six degrees of freedom (DoF) of the talocrural and subtalar joints [9]. However, most videofluoroscopic devices are stationary resulting in a limited field of view and therefore hindering the quantification of hindfoot kinematics throughout the complete stance phase [7–9]. Further, videofluoroscopy images only capture 2D information and time intensive 2D/3D registration of 3D bone geometries onto the 2D videofluoroscopy images is needed to acquire information about location and orientation of the individual bones in 3D. Recently developed advanced CT technologies allow to quantify individual bones throughout dynamic motion. By capturing the 3D spatial information accurate knowledge of 3D location and orientation of individual bones over time can be gained.

These 4D CT imaging systems are currently being successfully used to study dynamic activities in various joints [11]. For the foot-ankle complex, experimental studies have been performed in cadaveric [12,13], as well as healthy participants, and participants with foot-ankle pathologies [13–15] allowing differentiation between healthy and pathological talocrural and/or subtalar joint kinematics. However, these studies mainly focussed on clinical parameters such as syndesmotic distances or rotations of single bones during a limited, often manually induced motion. To our knowledge no study has yet analysed functional biomechanical parameters such as 3D hindfoot joint angles during a standardised complex motion representative of functional weight-bearing tasks like the stance phase of walking.

Beside information on joint kinematics, knowledge about articular joint mechanics (i.e. contact area and pressure) may be informative for understanding the structure-function relationship in both healthy participants and participants with a foot-ankle pathology. However, articular joint mechanics can currently not be measured *in vivo*. Previous *in vitro* studies have used pressure sensors inserted into the tibio-talar or talo-calcaneal joint space of cadaver specimens to measure articular joint mechanics during different loading scenarios [16–21]. Based on this data, *in silico* finite element analysis (FEA) [16] and discrete element analysis (DEA) [22–24] models have been developed and validated. While FEA studies are computationally expensive and limited to quasi-static analyses, DEA has been used to study contact area and pressure at the talocrural joint during motions comparable to the stance phase of walking [22,24]. However, these analyses separate the kinematic analysis from the assessment of articular joint mechanics, thereby reducing the complexity of the input kinematics for DEA by typically only accounting for talocrural plantar/dorsiflexion. Such simplifications are common in FEA and DEA, conversely musculoskeletal models can be used to study complete joint motion by accounting for all DoFs. This is particularly true for the hip and knee, but less for the foot-ankle complex where accurate representation of the anatomical structure is challenging. Early approaches modelled the foot-ankle complex with one [25] or two segments [26,27] and thereby oversimplified the anatomical structure, recent developments expanded the complexity of foot-ankle models by presenting models with an increased number of segments (up to 26 segments) [28–30]. By incorporating more segments and enabling motion in more DoF, a more accurate representation of the foot-ankle complex can be achieved, and assessments of individual motion of the talocrural and subtalar joints become possible. Ideally these musculoskeletal models are combined with articular cartilage representations to allow solving kinematics along with articular joint mechanics in a single model. Despite recent developments towards combining detailed musculoskeletal and contact models to study articular joint mechanics of the knee [31], most foot-ankle models are primarily rigid body models (i.e. without contact models), hindering their ability to estimate talocrural and subtalar articular joint mechanics. Only one model has been recently presented for the talocrural joint [32], however, this model does not contain an explicit cartilage geometry, instead modelling bone-on-bone contact.

Therefore, this work aims to explore the use of 4D CT imaging in combination with an innovative foot manipulator to capture detailed *in vivo* hindfoot kinematics during a simulated stance phase of walking and estimate talocrural and subtalar articular joint mechanics based on an *in silico* musculoskeletal foot-ankle model containing a complex and detailed representation of the bones, joints, and soft-tissues.

2. Methods

2.1. Participants

Twelve healthy participants (6♀/6♂, 29±10 years) were recruited for this study. All participants were injury-free during the last three month, had no history of previous foot-ankle injuries, and were physically active (>2 h of sports on a weekly basis). The study was approved by the local Medical Ethics Committee (S16464) and was performed in accordance with the Declaration of Helsinki. All participants read and signed an informed consent prior to the measurement.

2.2. Kinematic analysis

2.2.1. Foot manipulator

A unique CT-compatible foot manipulator (Fig. 1 A) was developed to impose plantar/dorsiflexion and inversion/eversion kinematics through its foot plate. Participants laid supine with their right foot attached to the foot manipulator and the ankle joint complex aligned with its axes of rotation. Through a tensioned strap system, participants applied load to the foot to ensure constant contact with the foot manipulator (Fig. 1B). The applied load was not monitored. The position of the foot manipulator was controlled by three linear actuators (LA30, 100 mm stroke, Linak, Nordborg, Denmark). The imposed movement was defined based on the stance phase of walking captured in one healthy volunteer using traditional marker-based motion capture (Fig. 1 C). It consisted of a range of motion (RoM) of 20.5° plantar/dorsiflexion (11.4° plantarflexion/9.1° dorsiflexion) and 8° inversion/eversion (5.6° inversion/2.4° eversion). The duration of the simulated stance phase was adapted to align with the image acquisition of the 4D CT scanner to a total duration of 10 seconds.

2.2.2. CT scans

All acquisitions were done on an Aquillion One CT scanner (Canon, Japan). A continuous sequence of 37–42 CT scans, each consisting of 320 slices (resolution 0.468×0.468 mm, slice thickness 0.5 mm), was captured at 3.6 Hz.

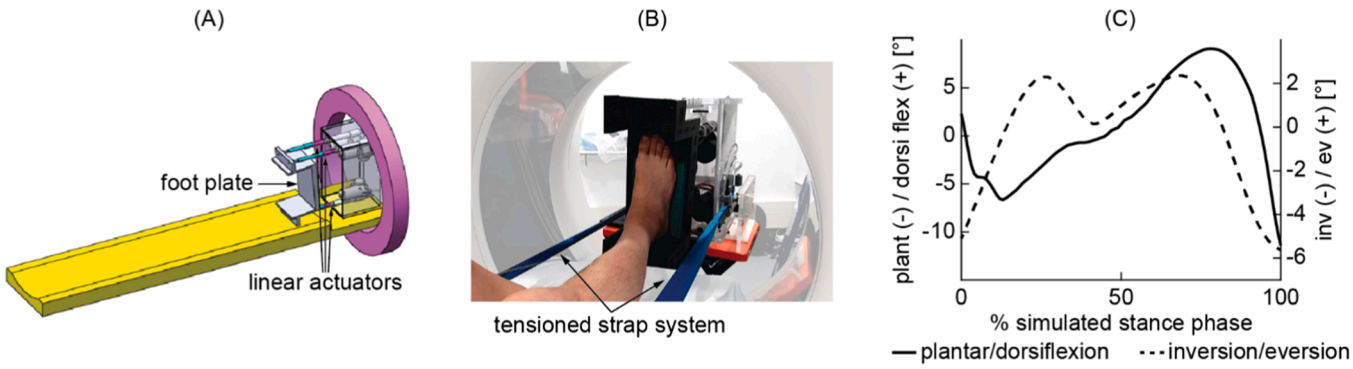

Fig. 1. (A) Detailed description of the foot manipulator, (B) position of the foot manipulator and a participants foot in the 4D CT scanner, (C) generic kinematic input template for plantar/dorsiflexion (plant/dorsi flex; solid line) and inversion/eversion (inv/ev; dashed line).

2.2.3. Joint rotations and translations

Geometries of the tibia, talus, and calcaneus were segmented in the initial time frame (Mimics Innovation Suite, Materialise NV, Belgium). Relevant anatomical landmarks were manually identified (3-matic, Materialise NV, Belgium) and bone specific anatomical coordinate systems defined [33]. The x-axis was defined from posterior towards anterior, the y-axis from distal towards proximal, and the z-axis from medial towards lateral, ensuring an orthonormal coordinate frame (Fig. 2). For all subsequent time frames, bone positions were calculated by first fitting the bone geometry of the first frame to each subsequent frame (Mimics Innovation Suite, Materialise NV, Belgium) and determining the consequent transformation matrices (MATLAB R2021b, The MathWorks Inc, United States). This approach has been previously used to quantify thumb motion in cadaveric specimens and has been validated using a cube with embedded silicon nitride beads [34]. Comparison of the resultant inter-bead distance during 4D CT scanning with the known machined distance achieved submillimetre precision (average difference 0.16±0.09 mm), and as such allows accurate reconstruction of 3D location and orientation of each foot bone over the simulated stance phase.

Based on the bone-specific transformation matrices and coordinate systems, talocrural and subtalar joint angles were calculated by projecting the vectors of the distal coordinate frame on the relevant planes of the proximal coordinate frame using a custom-made Matlab script (MATLAB R2021b, The MathWorks Inc, United States). Inversion/eversion was calculated as the angle between the projected distal y-axis on the proximal y-z plane and the proximal y-axis. Internal/external rotation was the angle between the projected distal z-axis on the proximal x-z plane and the proximal x-axis. Plantar/dorsiflexion was the angle between the projected distal x-axis on the proximal x-y plane and the proximal x-axis. Translations between adjacent segments were calculated relative to the proximal bones anatomical coordinate system (Fig. 2). Resultant rotations and translations were low pass filtered (2nd order Butterworth filter, 6 Hz cut-off frequency, MATLAB R2021b, The MathWorks Inc, United States), and normalised to the simulated stance phase. A neutral talocrural and subtalar joint configuration (i.e. with no rotations around the axes of rotation) was defined when the foot manipulator was in a neutral position and used as a reference point for further analysis. In addition, the talocrural and subtalar joint RoMs were calculated for each DoF.

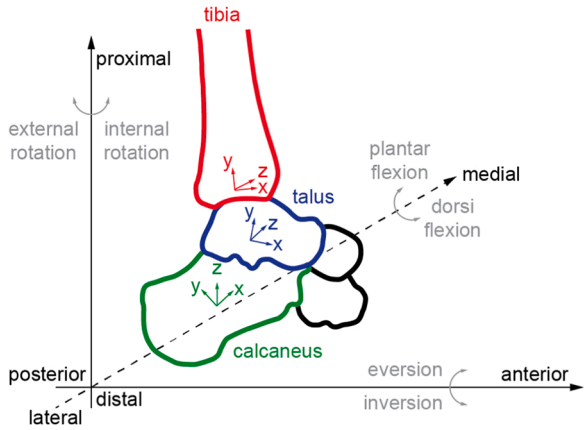

Fig. 2. Terminology used to describe talocrural and subtalar joint rotations and translations depicted in a right foot.

2.3. Musculoskeletal modelling

The KU Leuven extended foot-ankle musculoskeletal model [29] was adapted to each permit 6 DoF (3 rotations and 3 translations) at the talocrural and subtalar joint. Cartilage segmentations from a single healthy participant were morphed to fit the generic foot-ankle model geometries using a host-mesh fitting procedure [35]. A uniform 3 mm cartilage thickness was used for both joints. Articular contacts were implemented using an elastic foundation formulation based on cartilage stiffness and mesh penetration [31]. Cartilage parameters were based on a previously published knee model [31] but with adapted cartilage stiffness (elastic modulus: 10 MPa). Cartilage stiffness was adapted to be in line with previously published DEA and musculoskeletal modelling studies [22–24,32] and the mean cartilage Young's modulus specific to the ankle joint complex [36]. The base models' ligament and path actuators were supplemented with spring-like forces between the bones of the talocrural (tibia-talus) and subtalar (talus-calcaneus) joints. These were required as the updated model was insufficiently stabilised (i.e. producing non-physiological translations) when additional DoFs (i.e. talocrural: inversion/eversion, internal/external rotation, 3D translations; subtalar: flexion/extension, internal/external rotation, 3D translations) and the cartilage contact model were added. Parameters defining these springs were based on a previously published knee model [37] and can be found in the supplementary material (Table S 1).

For each participant, the generic foot-ankle model was combined with filtered participant-specific 4D CT based 3D rotations prescribed to the talocrural and subtalar joints in a forward simulation. Thereby, 3D translations were solved as a function of ligament, cartilage contact, spring-like, and passive muscle forces (OpenSim 4.3) [38,39]. Articular cartilage contact area and contact pressure were then estimated using the OpenSim joint articular mechanics (JAM) tool [31].

3. Results

3.1. Hindfoot kinematics

The imposed motion of the foot manipulator resulted in predominant plantar/dorsiflexion at the talocrural joint (RoM 15.9±3.9°), but

inversion/eversion at the subtalar joint (RoM 5.9±3.6°) (Fig. 3, Figure S 2). Inversion/eversion of the talocrural, plantar/dorsiflexion of the subtalar, and internal/external rotation for both joints, were small with individual RoM below 2.7°.

Along all three translational DoF, the calcaneus showed larger translations relative to the talus (subtalar joint) than the talus relative to the tibia (talocrural joint) (Fig. 4, Figure S 3). The calcaneus position was most posterior, distal, and lateral relative to the talus, when the talocrural joint was most plantarflexed, whereas peak anterior, proximal, and medial location occurred around maximum dorsiflexion.

3.2. Hindfoot articular joint mechanics

Throughout the simulated stance phase, the subtalar joint showed a larger joint contact area than the talocrural joint (Fig. 5 A, Figure S 4). At the beginning of the simulated stance phase, mean and maximum articular contact pressure were evenly distributed between the talocrural and subtalar joints (Fig. 5 A). During the first half of the stance phase, where the foot moved into plantarflexion, contact pressures were higher at the talocrural joint with a first peak talocrural contact pressure of 4.10±0.34 MPa at 13±8% of the simulated stance phase. After mid stance and with increasing dorsiflexion, articular contact pressure was redistributed from the talocrural to the subtalar joint with peak subtalar contact pressure of 4.50±0.53 MPa at 69±13% of the simulated stance phase. The overall largest contact pressure was found at the talocrural joint at the end of the simulated stance phase (4.90±0.36 MPa at 98 ±6%).

At the start of the simulated stance phase and with increasing plantarflexion, tibiotalar contact occurred on the posterior side of the talar cartilage. With increasing dorsiflexion, decreased contact pressure, and increased contact area, the tibiotalar contact moved anteriorly and more centrally (Fig. 5B). Talocalcaneal contact was distributed over an anterior-lateral and a posterior-medial contact area, with the anterior-lateral contact area experiencing higher pressure (Fig. 5B).

4. Discussion

4D CT scanning combined with an innovative foot manipulator allowed controlled and standardised acquisition of *in vivo* kinematics of the talocrural and subtalar joints during a simulated stance phase of walking. Combining this accurate kinematic data with a detailed *in silico* musculoskeletal foot-ankle model allowed estimating hindfoot articular joint mechanics and thus generate proof-of-concept *in vivo* data on articular contact area and contact pressure at the talocrural and subtalar joints during a dynamic functional motion.

Overall, comparability between participants and with literature assures that the imposed motion by the foot manipulator resulted in a motion similar to a healthy stance phase of walking. The motion of the foot manipulator resulted predominantly in talocrural plantar/dorsiflexion and subtalar inversion/eversion. The overall 3D rotational motion patterns of the talocrural and subtalar joint were comparable to previously published bone pin [2,4] and videofluoroscopy [8,40] data sets. Further, our findings of plantar/dorsiflexion and inversion/eversion predominantly occurring at the talocrural and subtalar joint, respectively, are in line with previous finding [7,9]. However, our participants presented reduced hindfoot RoMs for all rotational degrees of freedom [2,40], despite the fact that the imposed RoMs (plantar/-dorsiflexion 20.5°, inversion/eversion 8°) of the foot manipulator were in line with kinematic findings for the stance phase of healthy walking [2,40]. Further, two participants (participant 8 & 10, Figure S 2) showed contrary moving patterns, especially for plantar/dorsiflexion of the talocrural joint, potentially indicating that these two participants resisted the imposed motion of the foot manipulator. Despite this, the presented 4D CT measurement set-up provides a unique potential to assess functional motion of individual hindfoot bones in a fast and standardised manner that can be easily integrated in clinical practice for

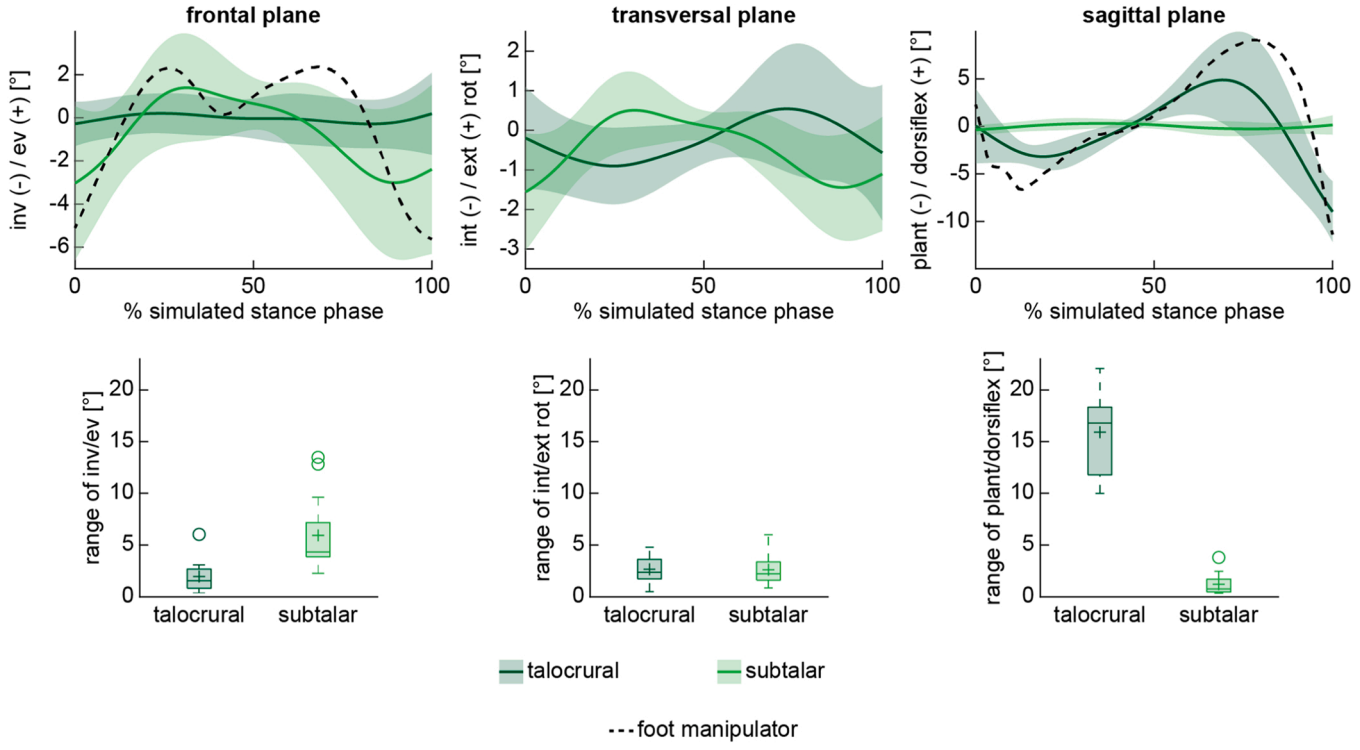

Fig. 3. Talocrural (dark green) and subtalar (light green) inversion/eversion (inv/ev, left), internal/external rotation (int/ext rot, middle), and plantar/dorsiflexion (plant/dorsi flex, right) throughout the simulated stance phase of walking. The average (thick lines) and standard deviations (shaded areas) for each joint are presented. In addition, the imposed motion of the foot manipulator is displayed (dotted black). Further the ranges of motion for each rotational degree of freedom are presented using box plots (below).

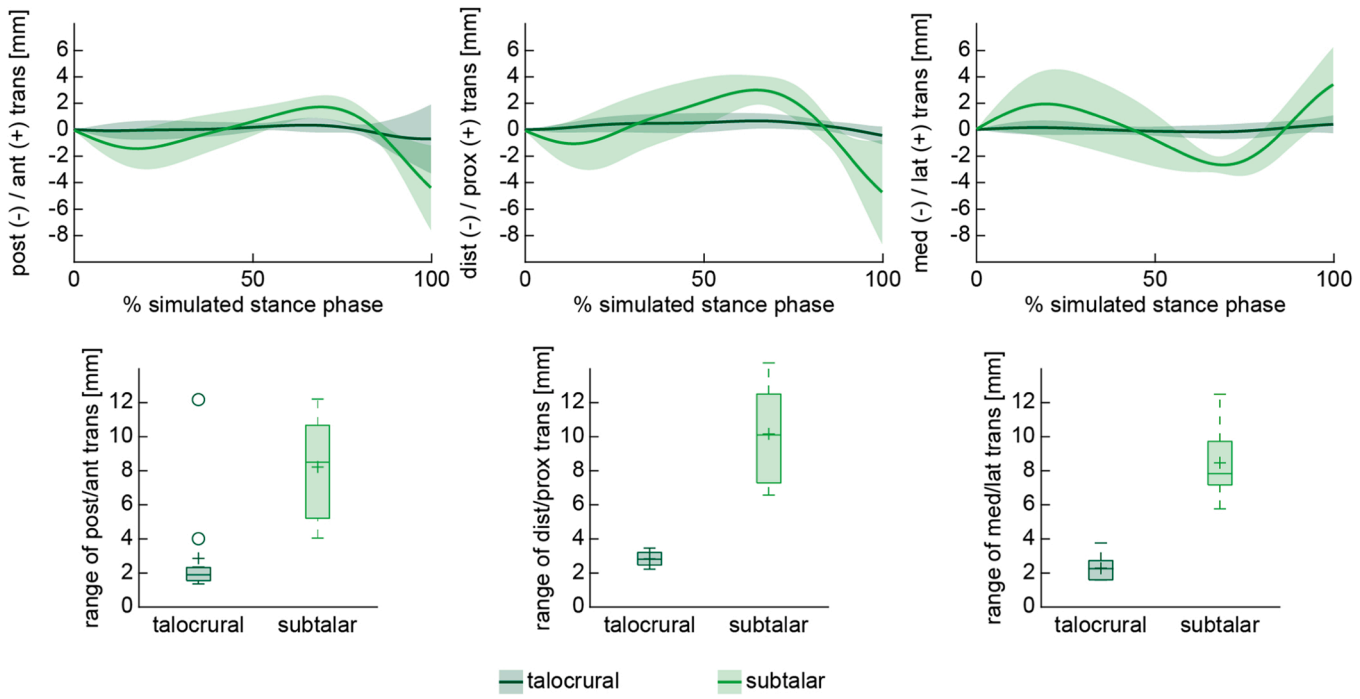

Fig. 4. Talocrural (dark green) and subtalar (light green) anterior/posterior (ant/post, left), proximal/distal (prox/dist, middle), and medio/lateral (med/lat, right) translations throughout the simulated stance phase of walking. The average (thick lines) and standard deviations (shaded areas) for each joint are presented. Further the ranges of motion for each translational degree of freedom are presented using box plots (below).

a wide range of patients.

Overall, talocrural joint contact area as well as mean and maximum contact pressure were strongly correlated with talocrural plantar/dorsiflexion, with contact area increasing from plantar to dorsiflexion, but mean and maximum contact pressure decreasing (Fig. 6). In general, contact locations of the hindfoot were in line with previously published *in vitro* measurements assessing articular contact locations using pressure sensitive films [16–21]. However, previously published results in general reported larger contact areas with maximal contact areas occurring at a neutral foot position and then decreasing for a plantarflexed as well as dorsiflexed position (Fig. 6) [18,19,41,42]. Nevertheless, the *in vitro* study of Millington and co-workers [43] as well as some specimens in the study of Matricali and co-workers [18] support our reported increase in contact area with increasing dorsiflexion. The reported observations in mean and maximal contact pressure, were in line with trends observed in *in vitro* studies using pressure sensors and FEA [16], but remained lower than other previously presented results [20, 22,23]. It should however be noted that these differences may be related to the fact that our contact mechanics result from simulations based on dynamic *in vivo* 3D kinematics of the talocrural and subtalar joints, whereas most *in vitro* measurements [16–20,43] or *in silico* simulations [22,23,43] consider a static plantar/dorsiflexion joint configuration. Furthermore, the applied axial loads varied strongly amongst the different studies (200 N [42] to 1360 N [20]). For our results on the subtalar contact area, only one other study was available for comparison [21] and here a slightly smaller contact area was found but with larger variations among participants.

To provide proof-of-concept data on clinical usability of this approach, identical 4D CT scanning and musculoskeletal modelling were used to evaluate the impact of an open reduction and internal fixation surgery of an intra-articular calcaneal fracture on hindfoot kinematics and articular joint mechanics of four participants (3♀/1♂, 44±19 years). Range of talocrural plantar/dorsiflexion was substantially reduced with almost no plantarflexion at the beginning of the simulated stance phase and a reduced peak dorsiflexion (Figure S 5). Further, subtalar joint RoMs were highly constrained, presenting almost no rotation in all three DoFs. The altered joint rotations also resulted in differences in the articular joint mechanics: Whereas the contact areas for both the talocrural and subtalar joints were comparable to the control participants at the beginning of the simulated stance phase, the in/decrease in contact area was reduced throughout the simulated stance phase (Figure S 6). This resulted in considerable decrease in mean and maximum contact pressures for the talocrural joint (first peak 3.80 ±0.37 MPa at 16±9% of the simulated stance and overall peak 4.44 ±0.33 MPa at the end of the simulated stance phase) as well as the subtalar joint (peak 3.93±0.15 MPa at 63±11% of the simulated stance phase). This comparison of a clinical cohort with our healthy participants provides evidence that the proposed workflow can identify meaningful differences in hindfoot kinematics and articular joint mechanics between healthy participants and participants with a foot-ankle pathology that need to be further investigated also in the light of the disappointing immediate clinical results often seen after calcaneal fracture fixation and the increased risk of cartilage degeneration on the longer term.

The presented analysis approach provides a comprehensive understanding of talocrural and subtalar joint kinematics and kinetics during a dynamic motion that can be implemented in clinical practise. However, specific limitations need to be considered. While the measurement set-up allowed analysis of a controlled and standardised motion, it does not allow analysis of free motion, nor the effect of compensatory movement strategies among participants. In addition, the analysed simulated stance phase was imposed over a duration of 10 s, compared to a healthy normal stance phase during dynamic walking of 0.6 s. With an increased scanning frequency, this could be improved and faster motions captured. In the current set-up, participants were asked to apply load to the foot manipulator to ensure constant contact, however, the magnitude of the applied load was not measured. Participants may have altered the magnitude of load applied to the foot manipulator throughout the simulated stance phase, potentially affecting (either limiting or exacerbating) the forces, and by extension the motion applied to the foot-ankle complex. In future studies, a load cell integrated in the measurement set-up can help to inform on the applied

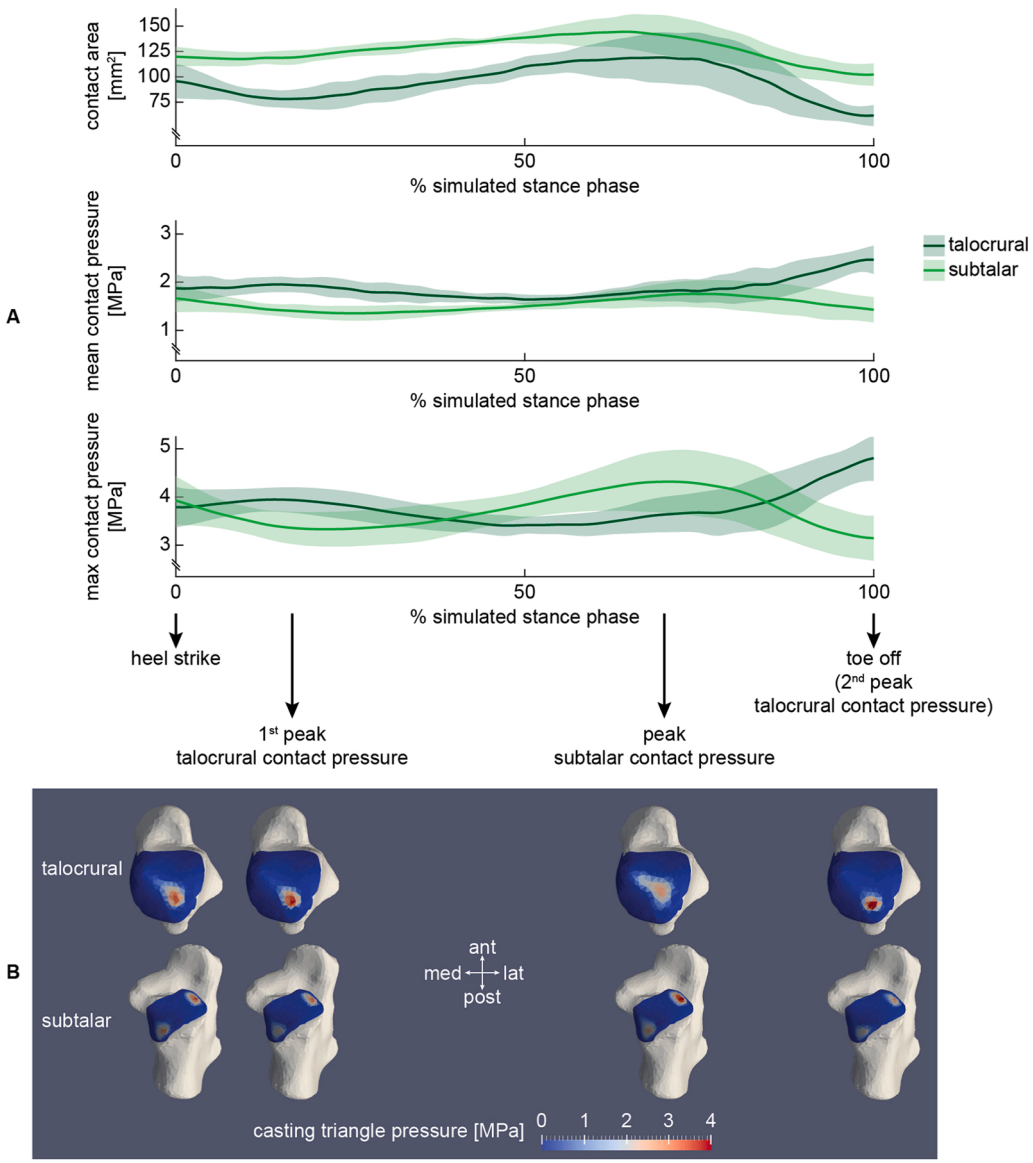

Fig. 5. (A) Talocrural and subtalar contact area (top), mean contact pressure (middle), and maximum (max) contact pressure (bottom) throughout the simulated stance phase of walking. The average (thick lines) and standard deviations (shaded areas) for each joint are presented. (B) Average articular contact pressure distribution of the talocrural joint projected on the talus (top) and subtalar joint projected on the calcaneus (bottom) across all participants at heel strike, 1st peak talocrural contact pressure, peak subtalar contact pressure, and toe off/2nd peak talocrural contact pressure.

loading magnitudes and the point of loading but also provide evidence if participants are resisting the imposed motion. The current workflow requires exposing participants to radiation (0.1 mSv), even though it being to more distal body parts of the body where radiation risk for internal organ damage is minimal. Lastly, the musculoskeletal model used was also limited in certain aspects. Spring-like forces were integrated between bones of the talocrural (tibia-talus) and subtalar (talus-calcaneus) joints to restrict non-physiological translations. While forces along the proximal/distal axis were minimal for both joints, higher forces occurred along the medio/lateral and antero/posterior axes. Spring-like forces were lower than those generated by muscles but exceeded generated ligament forces (Figure S 1). Future analyses should include a more complete set of soft-tissue structures which were not modelled here to alleviate the need for these spring-like forces. Further, the current study used a generic foot-ankle model which had a uniform cartilage thickness and was not scaled to individual foot size. Future developments of the musculoskeletal modelling workflow could incorporate more personalised anatomical structures (both in terms of bone geometries and articular cartilage geometries). Ultimately, the integration of dedicated pipelines to solve muscle force distribution e.g. using adapted static optimisation routines, needs to be considered to allow calculation of hindfoot articular joint mechanics while accounting for muscle forces during more active walking tasks.

5. Conclusion

Our study provides a detailed insight into hindfoot kinematics and kinetics during a dynamic motion comparable to walking. The used set-up combining *in vivo* 4D CT scanning with *in silico* musculoskeletal model-based simulations may be a feasible to implement approach to provide a comprehensive understanding of altered hindfoot function in clinical populations and its role in the pathomechanics associated with the onset and progression of degenerative joint diseases such as osteoarthritis.

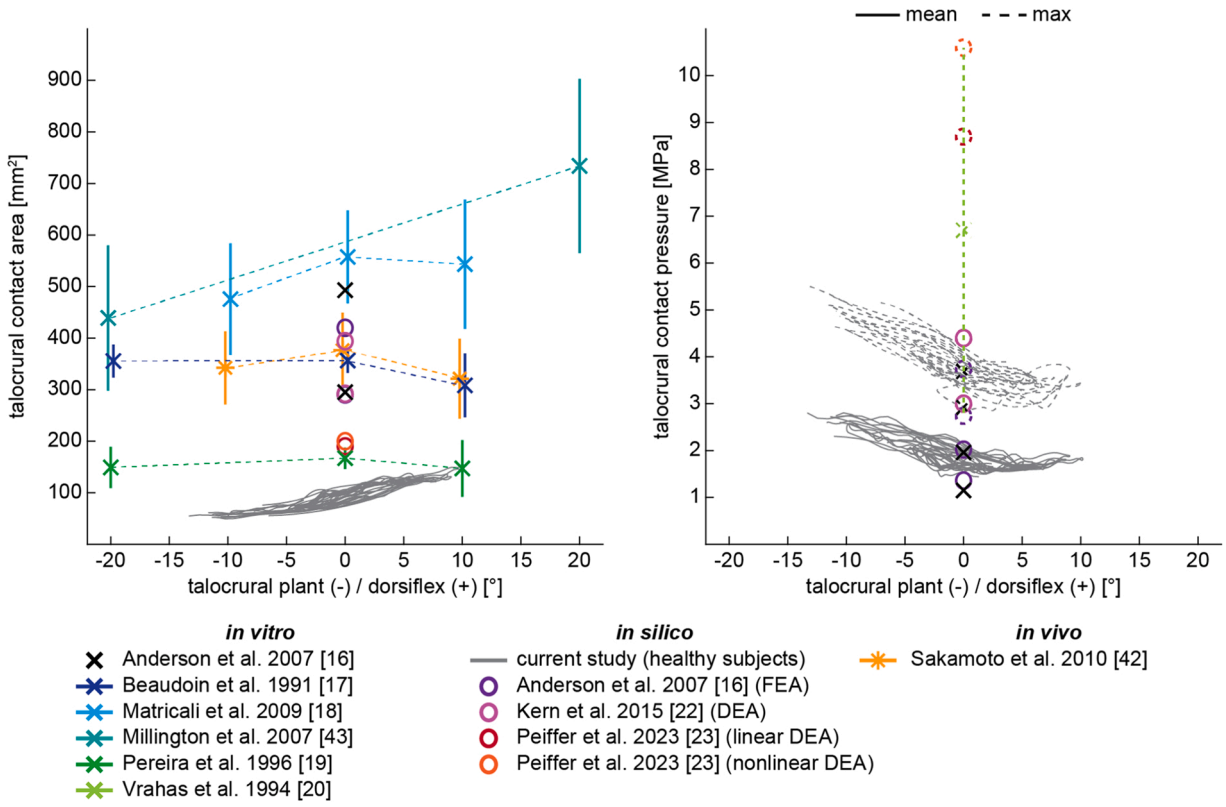

Fig. 6. Correlation of the talocrural contact area (left) and mean (solid line) and maximum (dashed line) contact pressure (right) versus talocrural plantar/dorsiflexion (plant/dorsiflex). Results for each individual of the 12 healthy participants are displayed. In addition, previously published mean ± standard deviations of in vitro, in silico (finite element analysis (FEA), discrete element analysis (DEA)), and in vivo measurements are presented.

CRediT authorship contribution statement

Barbara Postolka: Writing – review & editing, Writing – original draft, Visualization, Methodology, Investigation, Funding acquisition, Formal analysis, Data curation, Conceptualization. **Bryce A. Killen:** Writing – review & editing, Methodology, Formal analysis, Conceptualization, Data curation. **Hannelore Boey:** Writing – review & editing, Methodology, Investigation, Funding acquisition, Data curation. **Tiago M. Malaquias:** Writing – review & editing, Data curation. **Tassos Natsakis:** Writing – review & editing, Methodology, Data curation. **Stefan Clockaerts:** Writing – review & editing, Conceptualization. **Dominique Misselyn:** Writing – review & editing, Conceptualization. **Walter Coudyzer:** Writing – review & editing, Methodology, Data curation, Conceptualization. **Jos Vander Sloten:** Writing – review & editing, Funding acquisition, Conceptualization. **Ilse Jonkers:** Writing – review & editing, Supervision, Conceptualization, Funding acquisition, Project administration, Resources.

Declaration of Competing Interest

The authors declare the following financial interests/personal relationships which may be considered as potential competing interests: Barbara Postolka reports financial support was provided by the Swiss National Science Foundation [grant number 500PM 214210]. Hannelore Boey reports financial support was provided by the Research Foundation Flanders [grant number 1S36519N]. Jos Vander Sloten & Ilse Jonkers report financial support was provided by the Berghmans-Dereymaeker research chair on Foot & Ankle Biomechanics. The other authors declare to have no known competing financial interest or personal relationships that could have appeared to influence the work reported in this paper.

Acknowledgements

This work has been partially funded by a SNF Postdoc.Mobility fellowship (500PM 214210), the Research Foundation Flanders (1S36519N), and the Berghmans-Dereymaeker research chair on Foot & Ankle Biomechanics. The funding bodies were not involved in the data collection, nor the analysis or the interpretation of the data.

Appendix A. Supporting information

Supplementary data associated with this article can be found in the online version at doi:10.1016/j.gaitpost.2024.04.023.

References

[1] A. Cappozzo, F. Catani, A. Leardini, M.G. Benedetti, U. Della Croce, Position and orientation in space of bones during movement: experimental artefacts, Clin Biomech 11 (1996) 90–100.
[2] P. Lundgren, C. Nester, A. Liu, A. Arndt, R. Jones, A. Stacoff, P. Wolf, A. Lundberg, Invasive in vivo measurement of rear-, mid- and forefoot motion during walking, Gait Posture 28 (2008) 93–100.
[3] C.J. Nester, A.M. Liu, E. Ward, D. Howard, J. Cocheba, T. Derrick, P. Patterson, In vitro study of foot kinematics using a dynamic walking cadaver model, J Biomech 40 (2007) 1927–1937.
[4] A. Arndt, P. Westblad, I. Winson, T. Hashimoto, A. Lundberg, Ankle and subtalar kinematics measured with intracortical pins during the stance phase of walking, Foot Ankle Int 25 (2004) 357–364.
[5] B. Wang, K.E. Roach, A.L. Kapron, N.M. Fiorentino, C.L. Saltzman, M. Singer, A. E. Anderson, Accuracy and feasibility of high-speed dual fluoroscopy and model-based tracking to measure in vivo ankle arthrokinematics, Gait Posture 41 (2015) 888–893.
[6] J.N. Maharaj, S. Kessler, M.J. Rainbow, S.E. D'Andrea, N. Konow, L.A. Kelly, G. A. Lichtwark, S.E. D'Andrea, N. Konow, L.A. Kelly, G.A. Lichtwark, The reliability of foot and ankle bone and joint kinematics measured with biplanar videoradiography and manual scientific rotoscoping, Front Bioeng Biotechnol 8 (2020) 106.

[7] R.J. de Asla, L. Wan, H.E. Rubash, G. Li, Six DOF in vivo kinematics of the ankle joint complex: application of a combined dual-orthogonal fluoroscopic and magnetic resonance imaging technique, J Orthop Res 24 (2006) 1019–1027.
[8] S.E. Kessler, M.J. Rainbow, G.A. Lichtwark, A.G. Cresswell, S.E. D'andrea, N. Konow, L.A. Kelly, A direct comparison of biplanar videoradiography and optical motion capture for foot and ankle kinematics, Front Bioeng Biotechnol 7 (2019).
[9] K.E. Roach, B. Wang, A.L. Kapron, N.M. Fiorentino, C.L. Saltzman, K.B. Foreman, In Vivo kinematics of the tibiotalar and subtalar joints in asymptomatic subjects: a high-speed dual fluoroscopy study, J Biomech Eng 138 (2016) 1–9.
[10] K.J. Campbell, K.J. Wilson, R.F. LaPrade, T.O. Clanton, Normative rearfoot motion during barefoot and shod walking using biplane fluoroscopy, Knee Surg Sport Trauma Arthrosc 24 (2016) 1402–1408.
[11] L. Buzzatti, B. Keelson, J. Vanlauwe, N. Buls, J. De Mey, J. Vandemeulebroucke, E. Cattrysse, T. Scheerlinck, Evaluating lower limb kinematics and pathology with dynamic CT, Bone Jt J 103 (2021) 822–827.
[12] L. Buzzatti, B. Keelson, J. Apperloo, T. Scheerlinck, J.P. Baeyens, G. Van Gompel, J. Vandemeulebroucke, M. de Maeseneer, J. de Mey, N. Buls, E. Cattrysse, Four-dimensional CT as a valid approach to detect and quantify kinematic changes after selective ankle ligament sectioning, Sci Rep 9 (2019) 1291.
[13] P.A.G. Teixeira, A.S. Formery, A. Jacquot, G. Lux, I. Loiret, M. Perez, A. Blum, Quantitative analysis of subtalar joint motion with 4D CT: proof of concept with cadaveric and healthy subject evaluation, Am J Roentgenol 208 (2017) 150–158.
[14] P.A. Gondim Teixeira, A.S. Formery, G. Balazuc, G. Lux, I. Loiret, G. Hossu, A. Blum, Comparison between subtalar joint quantitative kinematic 4-D CT parameters in healthy volunteers and patients with joint stiffness or chronic ankle instability: a preliminary study, Eur J Radio 114 (2019) 76–84.
[15] M.T. Wong, C. Wiens, J. Lamothe, W.B. Edwards, P.S. Schneider, Four-dimensional CT analysis of normal syndesmotic motion, Foot Ankle Int 42 (2021) 1491–1501.
[16] D.D. Anderson, J.K. Goldsworthy, W. Li, M. James Rudert, Y. Tochigi, T.D. Brown, Physical validation of a patient-specific contact finite element model of the ankle, J Biomech 40 (2007) 1662–1669.
[17] A.J. Beaudoin, S.M. Fiore, W.R. Krause, R.S. Adelaar, Effect of isolated talocalcaneal fusion on contact in the ankle and talonavicular joints, Foot Ankle Int 12 (1991) 19–25.
[18] G.A. Matricali, W. Bartels, L. Labey, G.P.E. Dereymaeker, F.P. Luyten, J. Vander Sloten, High inter-specimen variability of baseline data for the tibio-talar contact area, Clin Biomech 24 (2009) 117–120.
[19] D.S. Pereira, K.J. Koval, R.B. Resnick, S.C. Sheskier, F. Kummer, J.D. Zuckerman, Tibiotalar contact area and pressure distribution: the effect of mortise widening and syndesmosis fixation, Foot Ankle Int 17 (1996) 269–274.
[20] M. Vrahas, F. Fu, B. Veenis, Intraarticular contact stresses with simulated ankle malunions, J Orthop Trauma 8 (1994) 159–166.
[21] C.L. Wang, C.K. Cheng, C.W. Chen, C.M. Lu, Y.S. Hang, T.K. Liu, Contact areas and pressure distributions in the subtalar joint, J Biomech 28 (1995).
[22] A.M. Kern, D.D. Anderson, Expedited patient-specific assessment of contact stress exposure in the ankle joint following definitive articular fracture reduction, J Biomech 48 (2015) 3427–3432.
[23] M. Peiffer, K. Duquesne, A. Van Oevelen, A. Burssens, S. De Mits, S.A.A. Maas, P. R. Atkins, A.E. Anderson, E.A. Audenaert, Validation of a personalized ligament-constraining discrete element framework for computing ankle joint contact mechanics, Comput Methods Prog Biomed 231 (2023) 107366.
[24] I. Benemerito, L. Modenese, E. Montefiori, C. Mazzà, M. Viceconti, D. Lacroix, L. Guo, An extended discrete element method for the estimation of contact pressure at the ankle joint during stance phase, Proc IMechE Part H J Eng Med 234 (2020) 507–516.
[25] J. Apkarian, S. Naumann, B. Cairns, A three-dimensional kinematic and dynamic model of the lower limb, J Biomech 22 (1989) 143–155.
[26] U. Rattanaprasert, R. Smith, M. Sullivan, W. Gilleard, Three-dimensional kinematics of the forefoot, rearfoot, and leg without the function of tibialis posterior in comparison with normals during stance phase of walking, Clin Biomech 14 (1999) 14–23.
[27] A.E. Hunt, R. M. Smith, M. Torode, A.M. Keenan, Inter-segment foot motion and ground reaction forces over the stance phase of walking, Clin Biomech 16 (2001) 592–600.
[28] J.N. Maharaj, M.J. Rainbow, A.G. Cresswell, S. Kessler, N. Konow, D. Gehring, G. A. Lichtwark, Modelling the complexity of the foot and ankle during human locomotion: the development and validation of a multi-segment foot model using biplanar videoradiography, Comput Methods Biomech Biomed Engin 25 (2022) 554–565.
[29] T.M. Malaquias, C. Silveira, W. Aerts, F. De Groote, G. Dereymaeker, J. Vander Sloten, I. Jonkers, Extended foot-ankle musculoskeletal models for application in movement analysis, Comput Methods Biomech Biomed Engin 20 (2017) 153–159.
[30] M. Oosterwaal, S. Carbes, S. Telfer, J. Woodburn, S. Tørholm, A.A. Al-Munajjed, L. van Rhijn, K. Meijer, The Glasgow-Maastricht foot model, evaluation of a 26 segment kinematic model of the foot, J Foot Ankle Res 9 (1) (2016) 10.
[31] C.R. Smith, K. Won Choi, D. Negrut, D.G. Thelen, Efficient computation of cartilage contact pressure with dynamic simulations of movement, Comput Methods Biomech Biomed Eng Imaging Vis 6 (2018) 491–498.
[32] T. Liu, A. Dimitrov, N. Jomha, S. Adeeb, M. El-Rich, L. Westover, Development and validation of a novel ankle joint musculoskeletal model, Med Biol Eng Comput (2024).
[33] M. Conconi, A. Pompili, N. Sancisi, A. Leardini, S. Durante, C. Belvedere, New anatomical reference systems for the bones of the foot and ankle complex: definitions and exploitation on clinical conditions, J Foot Ankle Res 14 (2021) 1–13.
[34] F.D. Kerkhof, E. Brugman, P. D'Agostino, B. Dourthe, G.H. van Lenthe, F. Stockmans, I. Jonkers, E.E. Vereecke, Quantifying thumb opposition kinematics using dynamic computed tomography, J Biomech 49 (2016) 1994–1999.
[35] J. Zhang, H. Sorby, J. Clement, C.D.L. Thomas, P. Hunter, P. Nielsen, D. Lloyd, M. Taylor, T. Besier, The MAP client: user-friendly musculoskeletal modelling workflows, Lect. Notes Comput. Sci. (Incl. Subser. Lect. Notes Artif. Intell. Lect. Notes Bioinforma.). 8789 (2014) 182–192.
[36] G.E. Kempson, The Mechanical Properties of Articular Cartilage, Academic Press, 1980.
[37] R.L. Lenhart, J. Kaiser, C.R. Smith, D.G. Thelen, Prediction and validation of load-dependent behavior of the tibiofemoral and patellofemoral joints during movement, Ann Biomed Eng 43 (2015) 2675–2685.
[38] S.L. Delp, F.C. Anderson, A.S. Arnold, P. Loan, A. Habib, C.T. John, E. Guendelman, D.G. Thelen, OpenSim: open-source software to create and analyze dynamic simulations of movement, IEEE Trans Biomed Eng 54 (2007) 1940–1950.
[39] A. Seth, J.L. Hicks, T.K. Uchida, A. Habib, C.L. Dembia, J.J. Dunne, C.F. Ong, M. S. DeMers, A. Rajagopal, M. Millard, S.R. Hamner, E.M. Arnold, J.R. Yong, S. K. Lakshmikanth, M.A. Sherman, J.P. Ku, S.L. Delp, OpenSim: simulating musculoskeletal dynamics and neuromuscular control to study human and animal movement, PLoS Comput Biol 14 (2018) e1006223.
[40] S. Cao, C. Wang, G. Zhang, X. Ma, X. Wang, J. Huang, C. Zhang, K. Wang, In vivo kinematics of functional ankle instability patients during the stance phase of walking, Gait Posture 73 (2019) 262–268.
[41] R. Stagni, A. Leardini, J.J. O'Connor, S. Giannini, F. Catani, S. Giannini, Role of passive structures in the mobility and stability of the human subtalar joint: a literature review, Foot Ankle Int 21 (2003) 602–615.
[42] M. Sakamoto, Y. Nodaguchi, Y. Tanabe, K. Sasagawa, Y. Kubota, H. Yoshida, K. Kobayashi, In Vivo contact areas of tibiotalar joint measured with magnetic resonance imaging, JSEM 10 (2010) 234–239.
[43] S. Millington, M. Grabner, R. Wozelka, S. Hurwitz, J. Crandall, A stereophotographic study of ankle joint contact area, J Orthop Res 25 (2007) 1465–1473.